Z. Physik 261, 283–304 (1973)

Elastic Scattering of ^{15}N on ^{19}F, ^{19}F on ^{18}O and ^{19}F on ^{16}O at Low Energies and Elastic Transfer

A. Gamp, W. von Oertzen*, H. G. Bohlen, M. Feil
R. L. Walter**, and N. Marquardt***

Max-Planck-Institut für Kernphysik, Heidelberg, W.-Germany

Received March 13, 1973

Angular distributions of the elastic scattering in the range of 30–160° θ_{CM} have been measured for the systems $^{15}N+^{19}F$, $^{19}F+^{16}O$ and $^{19}F+^{18}O$ at three energies, the highest being approximately 4 MeV above the Coulomb barrier. The large differences observed in the structure of the angular distributions at large angles are discussed considering elastic transfer, and the angular momentum balance for the possible direct surface reactions. The analysis yields a consistent description of the data in terms of elastic transfer.

I. Introduction

Extensive studies of elastic scattering of heavy ions on light nuclei [1–6] have shown that interesting information can be deduced from the data whenever strong deviations from an average behaviour, which is described by strong absorption, can be observed. These deviations are mainly observed at large angles, or at medium angles at higher incident energies, i.e. whenever the cross sections for the elastic scattering are small. The main phenomena responsible for deviations from a strong absorption scattering are, 1. weak absorption at the surface due to a lack of reaction channels which can carry away the incident angular momentum [3] (in these cases an enhancement of compound elastic contributions is observed and the excitation functions show fluctuations); and 2. transfer of the mass difference of the two colliding nuclei (elastic transfer) [4–6] which reproduces the incident channel and gives an enhancement of the cross section at large scattering angles.

In the present study the mass differences between the colliding nuclei range from 1 proton to four nucleons (α-particle). The additional proton in the $^{19}F+^{18}O$ system is a $2s_{1/2}$ nucleon which has a bound state wave function extending far out of the nucleus due to the one node. In the $^{19}F+^{16}O$ system a triton could be transferred, in the $^{15}N+^{19}F$ system

* Present address: Lawrence Radiation Laboratory, Berkeley, Calif.
** Permanent address: Duke University, Durham, North Carolina.
*** Now at: Laboratoire de Physique Nucléaire, Université de Montréal, Case postale 6128, Montréal 101, Canada.

an α-particle. There are also strong differences in the number of final reaction channels with positive Q-values. In all three systems, however, the number of final reaction channels with Q-values near zero seems to be sufficiently large to ensure strong absorption of the surface scattering waves (see Section IVa).

II. Experimental Technique

The experiments were performed using beams of ^{15}N (23–29 MeV) and ^{19}F (27–36 MeV) from the Heidelberg EN Tandem van de Graaff. Targets were LiF, CaF_2 for ^{19}F, SiO_2 for ^{16}O and NiO_2 for ^{18}O (60% ^{18}O, 40% ^{16}O content). The experimental requirements are characterized by a separation of nuclei of adjacent mass and charge. Using the technique of kinematical coincidences a mass separation can be achieved in the angular range of 50–120° θ_{CM}. If nuclei differ in charge it is more convenient to use $\Delta E-E$ telescopes. Thus in the case of $^{15}N+^{19}F$ and $^{19}F+^{16}O$ the angular distributions were measured using the proportional counter telescope [7] with Ar+Methan gas pressures of 30–50 mm Hg. The backward angles are obtained by measuring the recoil nuclei at small angles. The lower limit in angle is here determined by the ratio of elastic/recoil events which makes it necessary to reduce the beam intensity drastically to avoid large dead time at angles smaller 10° Lab. For forward scattering at small angles single counters with good resolution were used to get optimum separation from target contaminants. Spectra of recoiling ^{16}O nuclei from the bombardment of ^{16}O by ^{19}F are shown in Fig. 1, Fig. 2 shows spectra of ^{15}N on ^{19}F.

For the scattering of ^{19}F on ^{18}O a combination of $\Delta E-E$ telescope and kinematical coincidences was used [8]. The kinematical coincidence separates ^{16}O from ^{18}O which are both contained in the ^{18}O target. The $\Delta E-E$ relescope separates ^{16}O and ^{18}O from ^{19}F. This technique was necessary due to the fact that the separation of mass 18 from mass 19 necessitates very good angular resolution in certain angular regions (which would imply small solid angle). Simultaneous with the $\Delta E-E$ matrix (recorded in a two dimensional mode) gated by the kinematical coincidence the full $\Delta E-E$ spectrum was recorded. Projected spectra for oxygen, fluorine and ^{18}O (coincidence spectrum) are shown in Fig. 3.

Attempts were made to measure recoil ^{18}O nuclei at small angles in the reaction $^{19}F+^{18}O$ using a position sensitive detector in the focal plane of the Buechner magnetic spectrometer as applied to the $^{12}C+^{13}C$ and $^{13}C+^{14}C$ reaction [9]. However, at the low energies of the present experiment, at a vacuum of $1 \cdot 10^{-5}$ in the spectrometer, a large amount of events was observed at small angles, which is due to a change of charge state within the spectrometer of elastically scattered ^{19}F

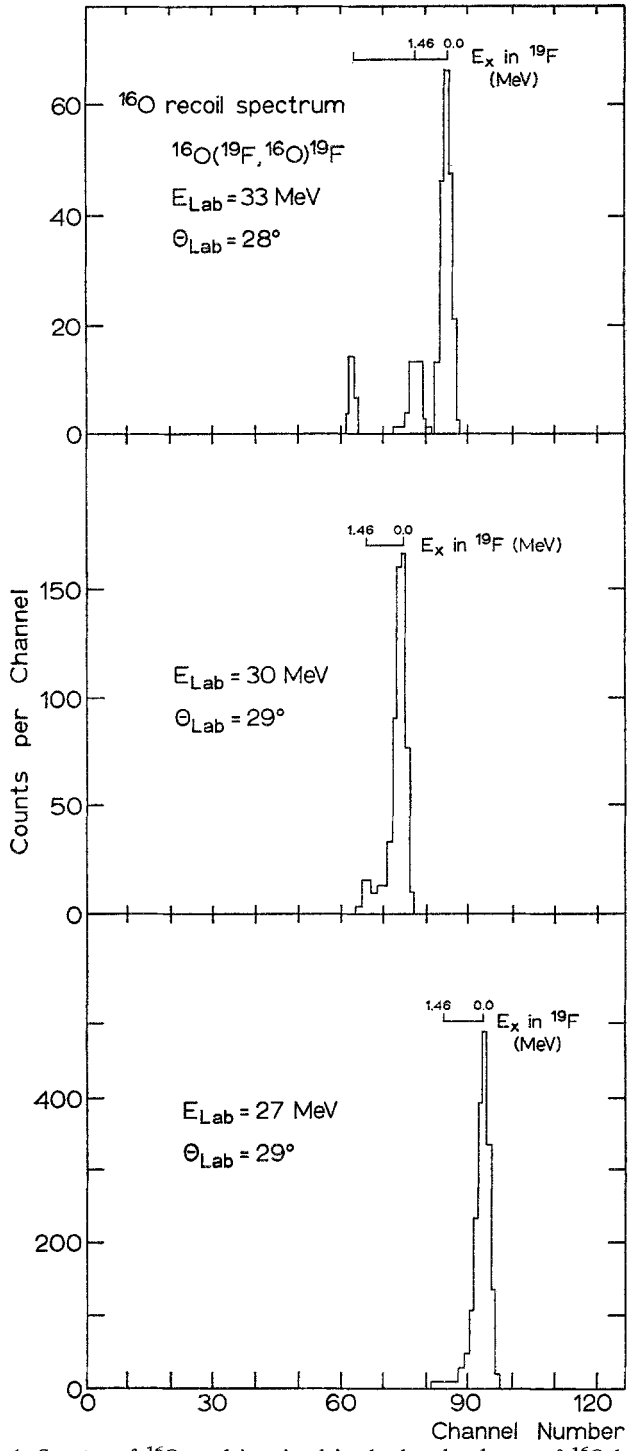

Fig. 1. Spectra of ^{16}O nuclei emitted in the bombardment of ^{16}O by ^{19}F

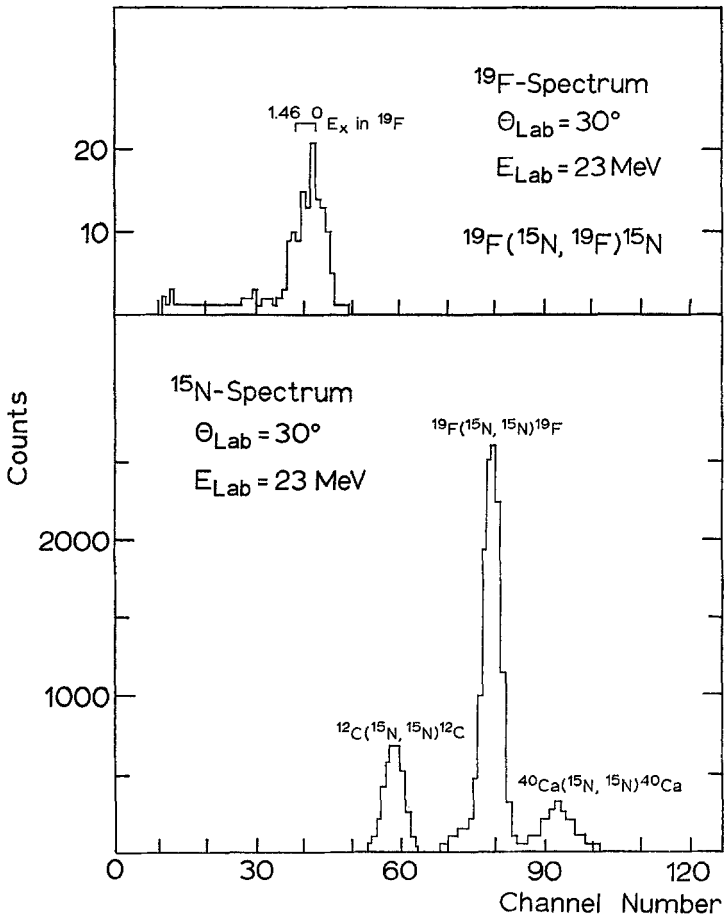

Fig. 2. Spectra of ^{19}F and ^{15}N nuclei emitted in the bombardment of ^{19}F by ^{15}N

($^{19}F^{7+} \rightarrow {}^{19}F^{8+}$). These particles identify on the focal plane as $^{18}O^{7+}$, making a clean measurement of ^{18}O recoil events impossible. The angular distributions of $^{19}F+{}^{18}O$ scattering therefore extend only to 130° CM as largest angle.

III. Experimental Results

The measurements for all three systems were performed using a two dimensional recording of ΔE and E measured with the proportional counter telescope. Inelastic scattering and reaction channels were measured therefore always simultaneously with the elastic scattering. At the

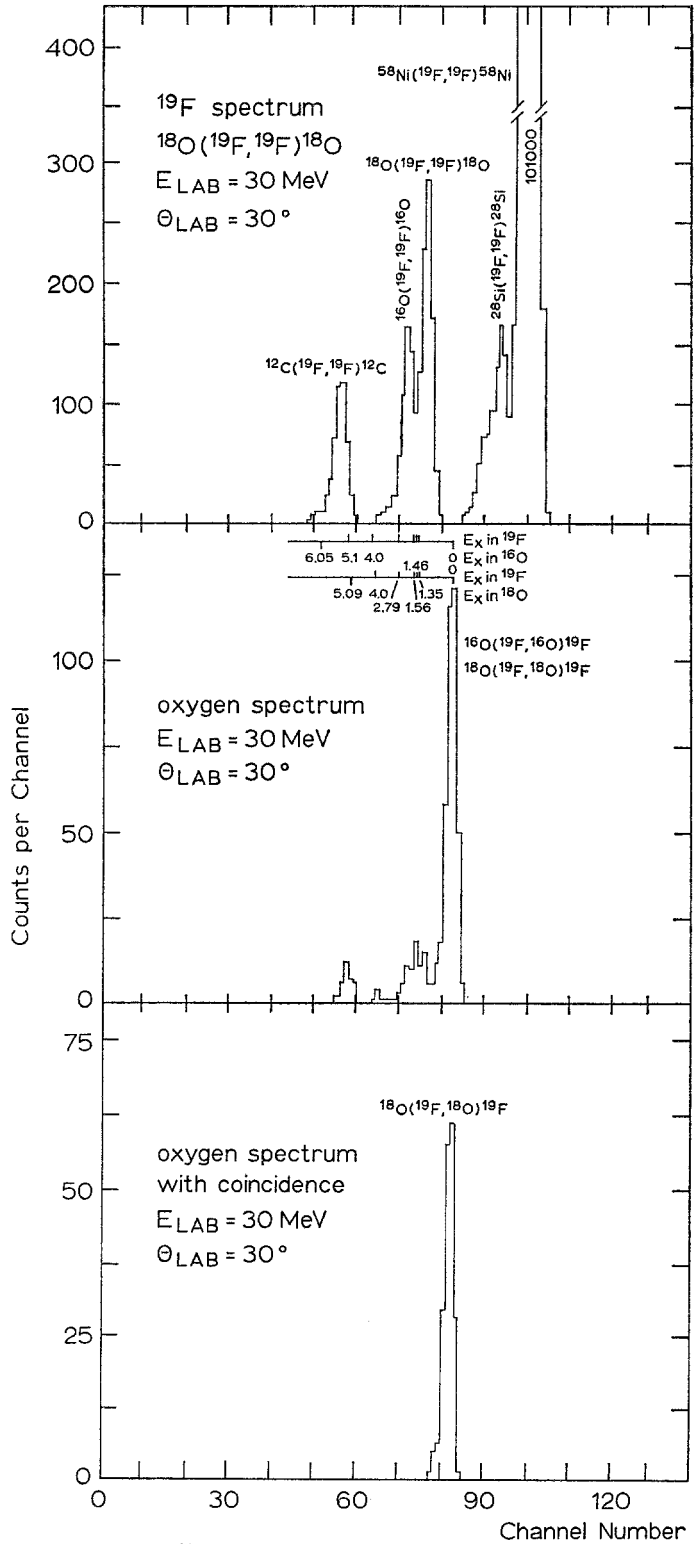

Fig. 3. Spectra of ^{19}F and oxygen nuclei in the reaction $^{19}F+^{18}O(^{16}O)$

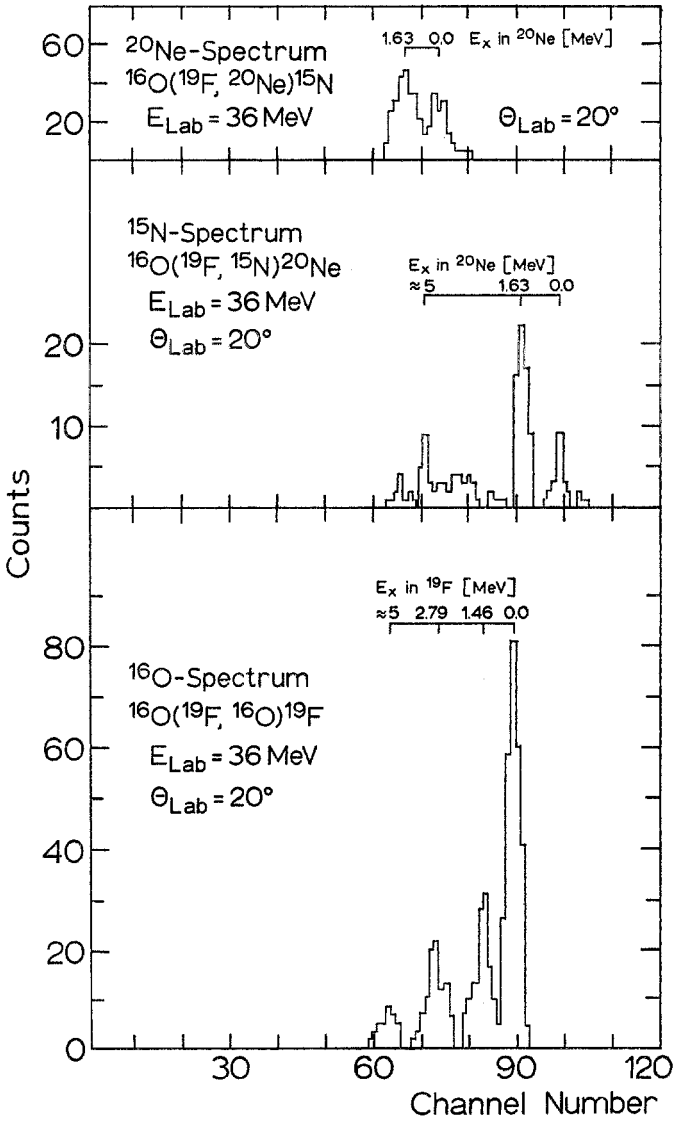

Fig. 4. Spectra of reaction products emitted in the reaction $^{19}F+^{16}O$ at 36 MeV

lower energies in all systems very few inelastic events and reactions were observed. At higher energies in all systems inelastic scattering (or inelastic transfer) to states of ^{19}F are observed. The energy resolution of 400–500 keV did not allow to separate the inelastic scattering to the low lying states in ^{19}F at ca. 150 keV excitation.

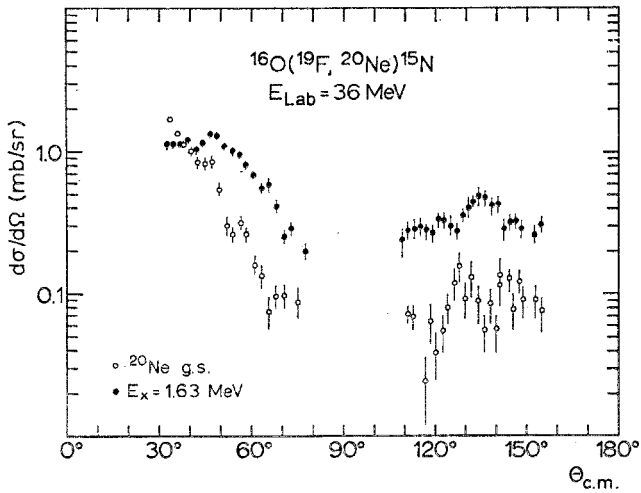

Fig. 5. Angular distributions of the reaction $^{16}O(^{19}F, ^{20}Ne)^{15}N$ at 36 MeV incident energy

a) $^{19}F+^{16}O$. Fig. 4 shows spectra of reaction products at the highest energy measured in the $^{19}F+^{16}O$ system. Proton transfer $^{16}O(^{19}F, ^{20}Ne)^{15}N$ and four particle transfer $^{16}O(^{19}F, ^{15}N)^{20}Ne$ are observed.

Angular distributions of this reaction at 36 MeV incident energy are shown in Fig. 5. At the lower energies the cross section was too small to give sufficient events during the present experiment.

Angular distributions of the inelastic scattering of ^{19}F on ^{16}O are shown in Fig. 6 at 33 and 36 MeV incident energies. Assuming that the two unresolved states at 100 and 200 keV excitation in ^{19}F are populated with comparable strength as the three levels at 1.5 MeV shown in Fig. 6, one could estimate a 10% contribution to the elastic scattering at large angles. This will result in a filling of the minima for angles larger 90° CM, which will appear less pronounced. At smaller angles the inelastic scattering at these energies gives a negligible contribution.

Angular distributions of the elastic scattering at 27, 30, 33 and 36 MeV are shown in Fig. 12 in Section IV. The pronounced structure observed at angles larger 90° CM stays at the same CM angles – as it is characteristic for an interference structure due to contributions from elastic transfer of a triton. Contributions from elastic transfer are therefore often difficult to observe in excitation functions, like for instance in the $^{16}O+^{18}O$ scattering [10].

b) $^{19}F+^{18}O$. In the scattering of ^{19}F on ^{18}O the inelastic scattering (or inelastic transfer) to the states at 1.5 MeV in ^{19}F is observed at the

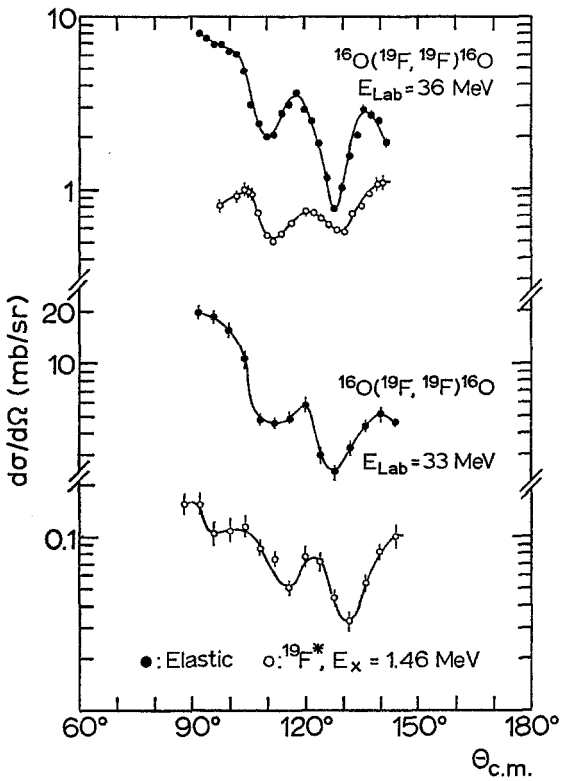

Fig. 6. Angular distributions of inelastic and elastic scattering (in absolute scale) for the scattering of ^{19}F on ^{16}O

higher energies too (Fig. 3). The excitation of the low lying states at 150 keV is again not separated. Their contribution to the elastic scattering, however, using the excitation strength of 1.5 MeV, is smaller than 5% at angles smaller than 90° CM and smaller than 10% at the largest angle measured, 130° CM. The inelastic scattering to the states at 150 keV thus will slightly fill the minima at larger angles and higher energy. Fig. 11 in Section IV.b shows the angular distributions at E_L=27, 30 and 33 MeV.

The pronounced structure observed in the region of θ_{CM} ranging from 90 to 160° retains again its position with energy. In this case the structure is produced by the interference of the elastic scattering with the proton transfer as discussed in the next section.

c) $^{15}N+^{19}F$. In the system ^{15}N+^{19}F the inelastic transitions to the states of ^{19}F at 1.5 MeV are rather weak. A considerable total yield of reaction products was observed in the ^{12}C and oxygen spectra (Fig. 7).

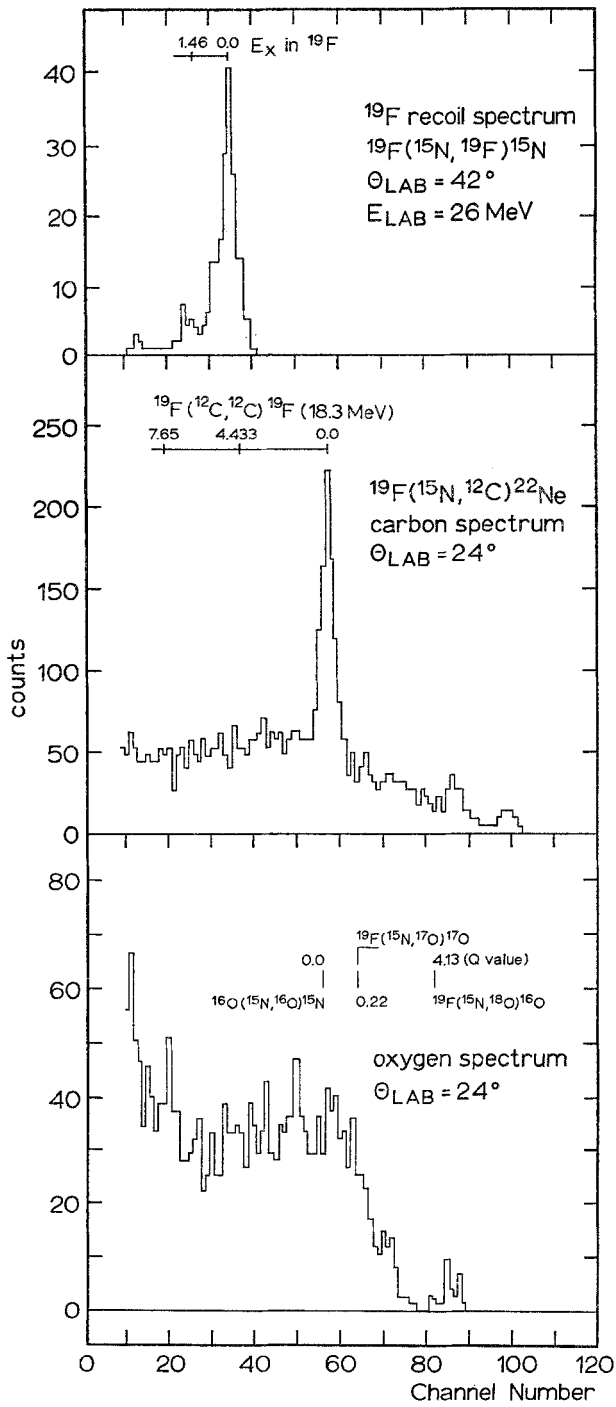

Fig. 7. Fluorine, carbon, oxygen spectra in the reaction $^{15}N + ^{19}F$; the strong ^{12}C line in b) is due to weak contamination of ^{12}C in the ^{15}N beam which was made at this energy using CN^- in the first stage of the *EN* Tandem

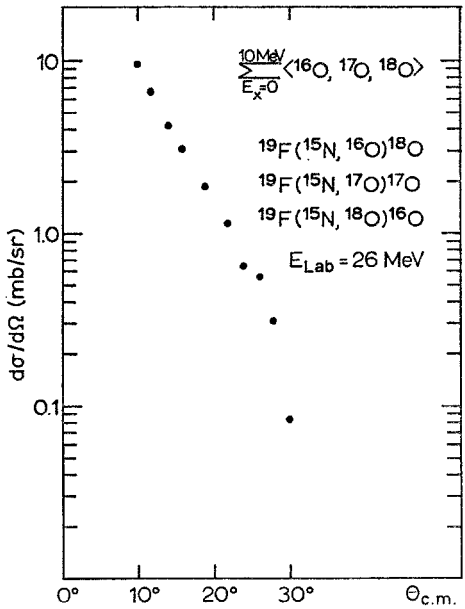

Fig. 8. Angular distribution of the total yield in the oxygen spectra in the reaction $^{15}N+^{19}F$

This yield was not observed in the ^{19}F spectrum, and could not be seen in the ^{15}N spectrum mainly due to the background which is always observed in the elastic (inelastic) spectrum. Fig. 8 shows the total (energy integrated) yield for the oxygen spectrum as function of angle. An exponentially rising yield is observed, whose interpretation is rather unclear.

The angular distributions (Fig. 13 in Sect. IV. b) of the elastic scattering are structureless and are comparable to those observed in the scattering of ^{19}F on ^{12}C [11]. The possible transfer of an α-particle seems to have no sizeable influence on the shape of the angular distribution.

IV. Analysis of the Data

1. Comparison of the Scattering of ^{15}N on ^{19}F, ^{19}F on ^{16}O and ^{19}F on ^{18}O

The general behaviour of the three different systems will be influenced by the number of final channels which can carry away the angular momentum brought into the compound system by the surface scattering waves, and by the strength of a possible elastic transfer.

The amount of absorption for the surface scattering waves is mainly influenced by the direct transfer and inelastic scattering channels [12], because there are usually still many states in the compound nuclei available for the surface angular momentum. Fig. 9 therefore gives the

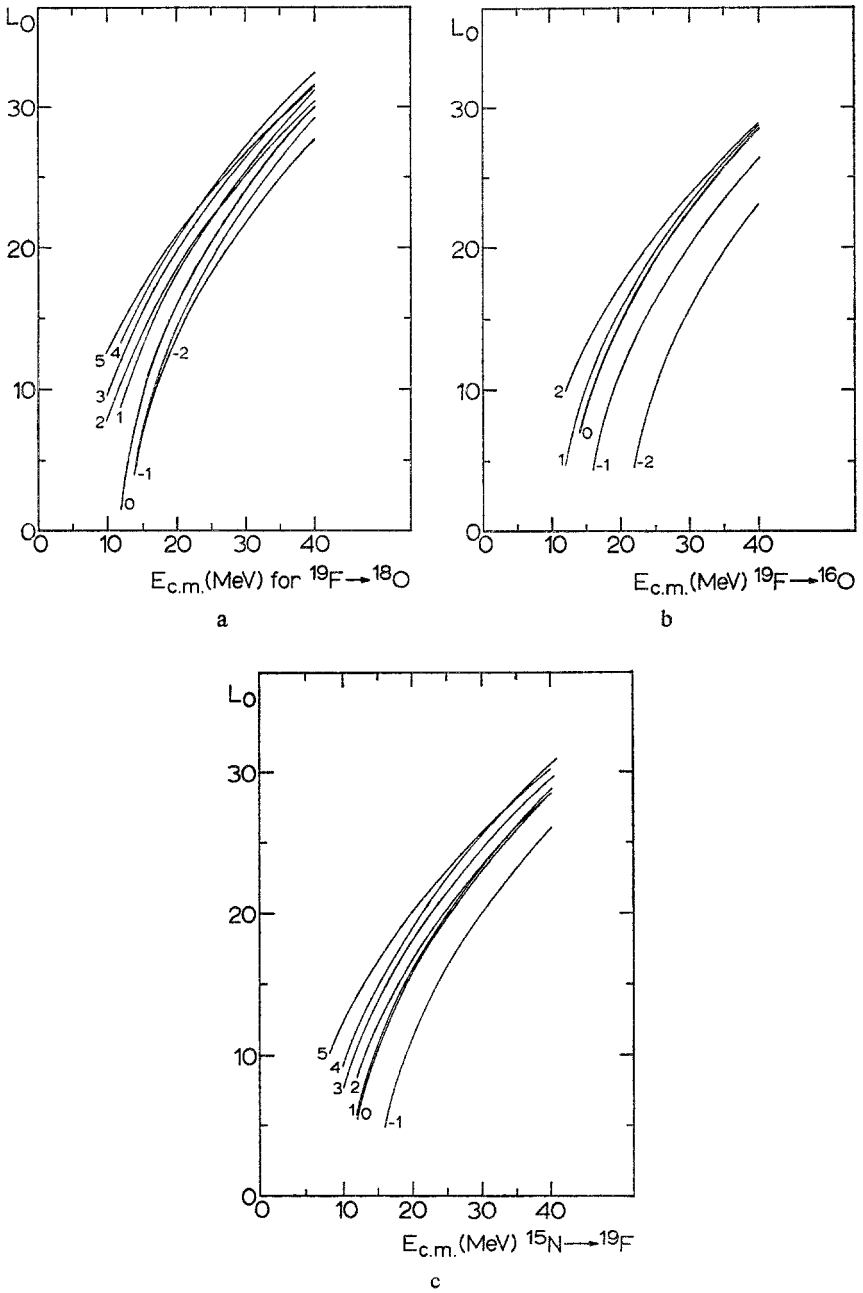

Fig. 9a—c. Grazing angular momenta L_0 for the incident channels (index 0) and several possible transfer channels for the systems $^{19}F+^{15}N$, $^{19}F+^{16}O$ and $^{19}F+^{18}O$

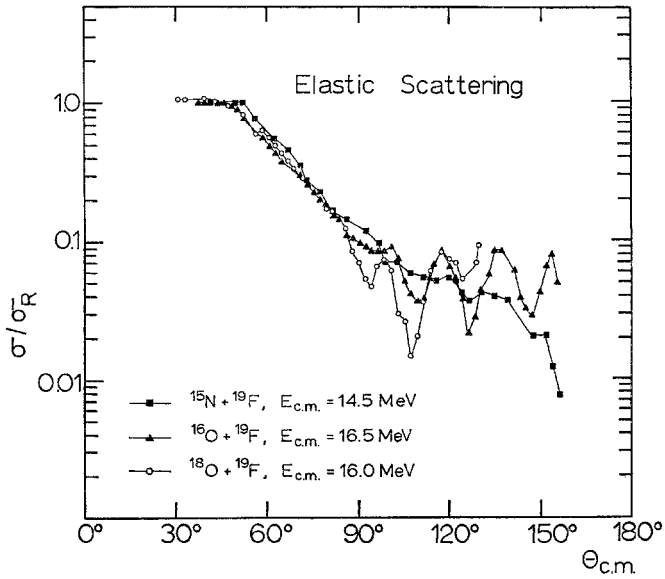

Fig. 10. Comparison of the elastic scattering of ^{15}N, ^{16}O and ^{18}O on ^{19}F at comparable center of mass energies (ca. 3 MeV above Coulomb barrier, for $^{15}N+^{19}F$ the Coulomb barrier is ca. 2 MeV lower)

grazing angular momenta L_0 for the incident channels in the three systems and for the possible transfer channels for each system. L_0 is calculated using the semiclassical expression

$$L_0(L_0+1)=k^2 R_0^2-2\eta kR_0$$

with

$$R_0=r_0(A_1^{1/3}+A_2^{1/3}) \qquad r_0=1.65 \text{ fm}.$$

One observes that for all systems there are reaction channels with positive Q-values, the $^{19}F+^{16}O$ system having the smallest number of available final channels.

A comparison of angular distributions of the three systems at comparable CM energies above the Coulomb barrier is shown in Fig.10. The decrease of the differential cross section from $\sigma/\sigma_R \approx 1$ to the ratio of 0.1 is nearly the same for all three systems indicating that the amount of absorption of the surface partial waves is approximately the same. Actually, a certain absorption at the surface of the nucleus can not be surpassed by stronger absorption because the amplitudes of the scat-

tering waves become quickly rather small and insensitive to differences in the real and imaginary potentials. We may conclude that all three systems have rather strongly absorbing potentials (which is directly deduced for $^{19}F+^{18}O$ and $^{15}N+^{19}F$ from Fig. 9). Inelastic transitions to states in ^{19}F at 150 keV and 1.5 MeV, which can occur in all three systems (as discussed in the previous section) will also tend to make the three systems rather similar. The differences observed in the three systems studied in this work will therefore be due to differences in the strength of the contribution of elastic transfer as discussed in the following Sections IV.b.

2. *Elastic Transfer in the Elastic Scattering of ^{19}F on ^{18}O, ^{16}O and ^{15}N on ^{19}F*

a) A Semiclassical Model for the Elastic Scattering with Elastic Transfer. The scattering of two nuclei A und B with $B=A'+C$ consisting of a core A' identical to A; $(A\equiv A')$ will be described by two possible amplitudes

$f_{el}(\theta)$ – elastic scattering, $A(B, B)A$

$f_{tr}(\pi-\theta)$ – transfer of particle C, $A(B, A)B$.

The total amplitude is $|f_{el}(\theta)+(-)^A(-)^{\ell}f_{tr}(\pi-\theta)|^2=|f_t|^2$. The sign $(-)^A$ takes into account whether the cores A are bosons or fermions and $(-)^{\ell}$ carries a sign due to the bound state wave function of particle C with angular momentum ℓ [6, 13]. The coherent addition of these two amplitudes leads to similar interference phenomena observed in the scattering of really identical nuclei. We describe $f_{el}(\theta)$ by a Rutherford scattering with absorption described by a function $f_{abs}(\theta)$

$$f_{el}(\theta)=f_R(\theta)\cdot f_{abs}(\theta)=\frac{a}{\sin^2\theta/2}\,e^{-i\eta\ln\sin^2\theta/2}\cdot f_{abs}(\theta)$$

$a=\dfrac{\eta}{2k}$, $\eta=$ Sommerfeldparameter,

$k=$ wave number of relative motion.

For the transfer amplitude we write in the semiclassical approximation [14]

$$f_{tr}(\pi-\theta)=f_{el}(\pi-\theta)\cdot P_{tr}(\pi-\theta)$$

with $P_{tr}(\pi-\theta)$ being the transfer probability. We thus obtain

$$\frac{d\sigma}{d\Omega}=|f_t(\theta)|^2=\frac{f_{abs}^2(\theta)\,a^2}{\sin^4\theta/2}+\frac{a^2 P_{tr}^2 f_{abs}^2(\pi-\theta)}{\cos^4\theta/2}$$
$$+(-)^A(-)^{\ell}\frac{2a^2 P_{tr}(\pi-\theta)f_{abs}(\pi-\theta)}{\sin^2\theta/2\cos^2\theta/2}\cos(\eta\ln\mathrm{tg}^2\theta/2+\delta).$$

This expression gives a particular simple picture of the phenomena which will be observed in systems where elastic transfer occurs. If the transfer probability would be constant and equal to unity, we should observe Mott-scattering with equal cross sections at angles θ and $(\pi-\theta)$ and the typical interference term which gives rise to strong oscillations around 90° CM with a frequency determined approximately by η due to the term $\cos(\eta\ln\mathrm{tg}^2\theta/2)$. Given a certain transfer probability P_{tr}, and in particular a certain dependence of $P_{tr}(\theta)$ on the distance of closest approach, i.e. scattering angle, we will observe interference structures in the angular region, where $f_{tr}(\pi-\theta)$ and $f_{el}(\theta)$ become comparable. Illustrations of these facts are shown in Fig. 14 where the non interfering cross sections and the total cross section are shown. Again the frequency of the oscillations observed in the angular distributions is given by the Sommerfeld parameter η. The parameter η is 9 for ^{19}F on ^{18}O, ^{16}O, corresponding to a distance between two maxima of $180°/\eta\approx 20°$ which is in very good agreement with the experimental results.

b) Analysis of the Data in the Molecular two State Approximation. The elastic scattering with elastic transfer can be conveniently described (for system with small intrinsic spin and angular momentum of the transferred particle) using the method of molecular wave function in a two state approximation [6, 13, 14]. In this method the total wave function of the system Ψ is expanded in terms of molecular scattering states of the transferred particle $C\,\Phi(R, r)$ which are a function of the distance between the two cores R

$$\Psi(R, r)=\sum\chi(R)\Phi(R, r).$$

$\chi(R)$ are scattering wave functions defined by the solution of the corresponding Schroedinger equation. The expansion can be restricted to two states. They consist of a linear combination of the unperturbed identical ground states, in which the transferred particle is bound to either one of the two cores. Thus a particular simple solution for the total scattering amplitude is obtained [6, 13].

The Schroedinger equation for the scattering process in this description contains a general optical (complex) potential $V_{opt}(R)$ and a potential term given by the energy of the molecular state $\langle \Phi_p | h | \Phi_p \rangle = E_p(R)$

$$\left(-\frac{\hbar^2}{2m} V_R^2 + V_{opt}(R) + (-)^{A+\ell} p E_p(R) - E_{CM}\right) \chi_p(R) = 0.$$

If the system has more states directly coupled, the two-state-approximation (which is the essential approximation) leads to an imaginary part of $E_p(R)$ [15]. The partial waves are separated into those with even and odd parity ($p = \pm 1$) corresponding to the property of the two molecular scattering states, which are either even or odd under the interchange of the two identical cores (operation P) $P\Phi_p = p\Phi_p(-)^{A+\ell}$, $p = \pm 1$. An additional sign appears which takes into account the boson or fermion property of the identical cores $(-)^A$, and the intrinsic parity of the bound state with angular momentum ℓ, $(-)^\ell$ [14]. The even and odd partial waves are submitted to different total potentials, due to the sign in the additional potential term, and the structure observed in the angular distributions depends on two main properties [13]

1. the cores are bosons or fermions,

2. the angular momentum ℓ of the bound state wave function is even or odd.

In the analysis the complex optical potential was chosen to be of the standard Woods-Saxon form $V = V(R) + i W(R)$ with

$$V(R) = V_0 / (1 + \exp\{(R - R_0)/a_0\})$$

and

$$W(R) = W / (1 + \exp\{(R - R_i)/a_i\}).$$

The radii are defined as usual by a radius parameter $r_{0,i}$:

$$R_{0,i} = r_{0,i}(A_1^{1/3} + A_2^{1/3}).$$

The energy of the molecular scattering states $E_p(R)$, which acts as an additional exchange potential has a Yukawa form at the large distances which are important in the scattering of strongly absorbed particles [6]. $R > R_{int}$.

$$E_p(R) \sim (SN)^2 \frac{E_B}{\alpha^3} \frac{e^{-\alpha R}}{\alpha R}$$

with

$$\alpha = \sqrt{2 m E_B \hbar^{-2}}.$$

Here S is the spectroscopic amplitude for the exchange particle in the bound state representing nucleus B in its ground state. (S^2-spectroscopic factor); and N gives the normalization of the bound state wave function with respect to an equivalent Hankel function at the nuclear surface (i.e. outside the strong interaction region). The normalization constant N is obtained by calculating the bound state wave function in an appropriate Woods-Saxon potential.

$^{19}F+^{18}O$. For the case ^{19}F+^{18}O the complex potential could be taken from the ^{18}O+^{18}O scattering [12]. Adjusting the strength parameter SN a very good description of the data was obtained immediately as shown in Fig. 11. The relevant parameters are compiled in Table 1 with those for the other cases. Although better fits to the individual angular distributions are possible preference was given to parameter sets which give comparable good description at all energies. The strength parameter SN obtained from the experiment is slightly energy dependent, which could be mainly due to the fact that the description of the bound state wave function by a single Hankel function is not adequate for a proton. The constant N thus depends not only on bound state potential parameters (which were chosen to have standard values as used in (^{3}He, d). The value of the spectroscopic factor obtained $S^2=0.36$ is in good agreement with those obtained from other experiments (^{3}He, d) as $S^2=0.42$ [16] and $S^2=0.45$ [17].

It is important to note that the correct phase of the structure is reproduced only if the even partial waves are submitted to the attractive exchange potential, a fact which is determined by the $(-)^{A+t}$ sign (particle C is a $2S_{1/2}$ proton) and thus opposite to the findings in systems from the $1p$ shell like ^{12}C+^{13}C [14].

Further, unresolved transitions to states in ^{19}F at 150 keV add only incoherently to the differential cross section and have no influence on the size of the oscillations (they may, however, slightly fill the minima). The scattering of ^{19}F on ^{18}O thus gives an interesting example of the possibilities of elastic transfer: spectroscopic information can be deduced for a state which is not separated from the adjacent states, because its reaction amplitude is amplified by its interference with elastic scattering. The important information is contained in the phase and amplitude of the oscillation. The same observation is applicable to the next cases ^{19}F+^{16}O and ^{19}F+^{15}N.

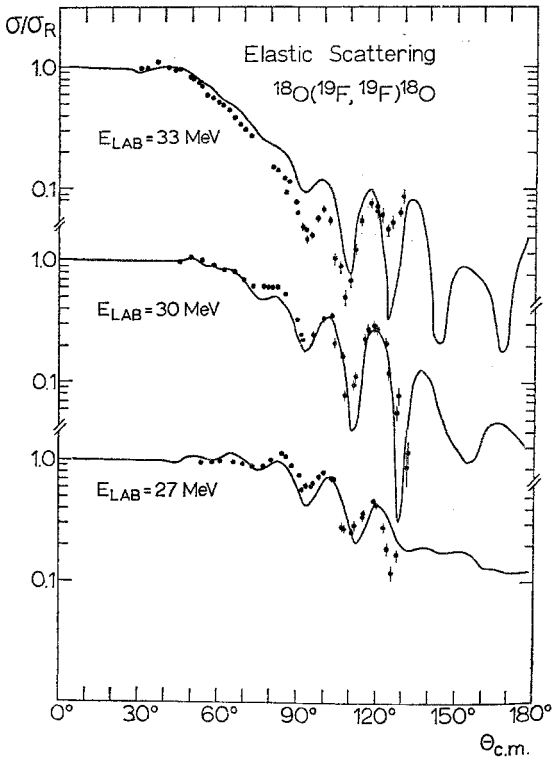

Fig. 11. Angular distributions of the elastic scattering of ^{19}F on ^{18}O. The solid lines are calculations using the molecular two-state-approximation for the elastic transfer (parameters are given in Table 1)

Table 1. Optical model parameters r_0, a_0, r_i, a_i, V, W, S^2 = spectroscopic factor

System	E_{LAB} MeV	r_0 fm	a_0 fm	r_i fm	a_i fm	V MeV	W MeV	SN	N	S^2	E_{CM} MeV
$^{19}F+^{18}O$	33	1.33	0.45	1.25	0.57	17	7.0	2.08	4.84	0.176	16.0
	30	1.33	0.45	1.25	0.57	17	6.5	2.85	4.84	0.35	14.6
	27	1.33	0.45	1.25	0.57	17	6.0	3.0	4.84	0.38	13.1
$^{19}F+^{16}O$	36	1.34	0.47	1.25	0.57	17	9	111	205	0.29	16.45
	33	1.34	0.47	1.25	0.57	17	9	115	205	0.31	15.08
	30	1.34	0.47	1.25	0.57	17	9	111.8	205	0.29	13.71
	27	1.34	0.47	1.25	0.57	17	9	112.6	205	0.3	12.34
$^{15}N+^{19}F$	29	1.33	0.5	1.25	0.57	17	10	15.35	71	0.049	16.2
	26	1.33	0.5	1.25	0.57	17	10	15.0	71	0.049	14.53
	23	1.33	0.5	1.25	0.57	17	10	15.0	71	0.049	12.85

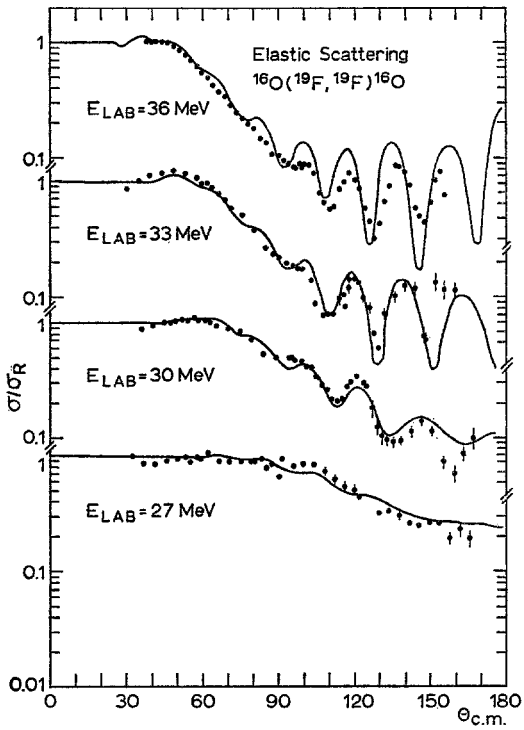

Fig. 12. Angular distributions of the elastic scattering of ^{19}F on ^{16}O. The solid lines are calculations using the molecular two-state-approximation for the elastic transfer of the triton (parameters in Table 1)

$^{19}F+^{16}O$. In the scattering of ^{19}F + ^{16}O the transfer of a triton can occur. Fig. 12 shows the experimental angular distributions and calculations which include the elastic transfer of the triton (parameters are given in Table 1). The normalization constant N for the triton was obtained using the same parameters for the bound state potential which were used in the analysis of triton the transfer reaction ^{16}O(^{7}Li, α)^{19}F [18] ($r_0 = 1.7$ fm, $a = 0.7$ fm). The spectroscopic factor for the triton $S^2 = 0.29$ obtained from the present calculation agrees well with the value obtained from the ^{7}Li induced reaction, $S^2 = 0.2$ (Ref. [18]). Again, as discussed for the case ^{19}F + ^{18}O the extraction of the spectroscopic information for the ^{19}F ground state does not depend on the fact that the ground state is separated from its adjacent states and does not depend on an absolute value of the cross section, but on the position and strength of oscillatory structure in the angular distribution.

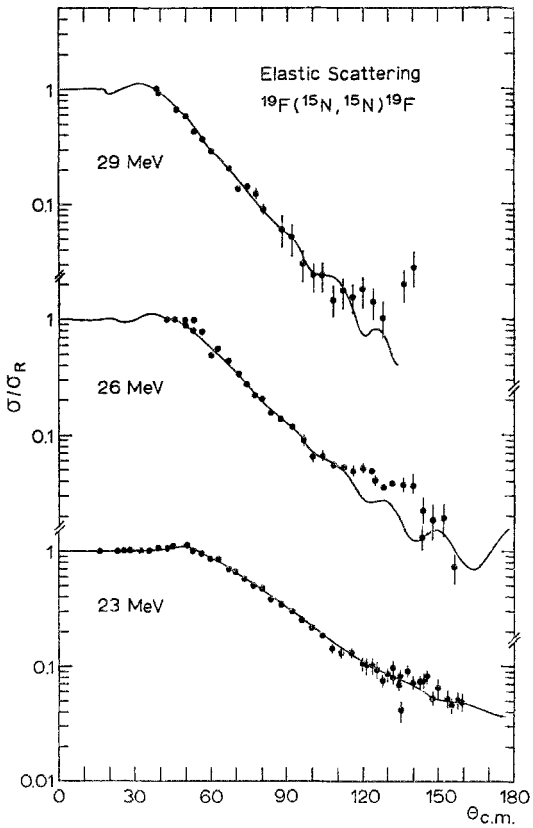

Fig. 13. Angular distributions of the elastic scattering of ^{15}N+^{19}F. The solid lines are calculations using the molecular-two-state approximation for the elastic transfer of the α-particle (parameters in Table 1)

$^{19}F+^{15}N$. The angular distributions of the scattering ^{19}F+^{15}N do not show any structure (Fig. 13). The rather small binding energy of the α-particle in ^{19}F of only ~4.0 MeV would suggest that transfer of an α-particle could be rather probable. The absence of structure in the angular distributions thus sets an upper limit to the spectroscopic factor for the α-particle in ^{19}F. Again the parameters given in Ref. [18] in the analysis of the ^{15}N(^{7}Li, t)^{19}F reaction were used for the calculation of the bound state wave function of the α-particle in ^{19}F. The upper limit for the spectroscopic factor obtained from the calculations shown in Fig. 13 is approx. $S^2=0.06$ (the remaining parameters are given in

Table 1). The value obtained in Ref. [18] from the analysis of the ^{7}Li induced reaction is $S^2=0.088$ in rather good agreement with the result of the present analysis.

V. Conclusions

The elastic scattering of ^{19}F is well described by rather strongly absorbing potentials (see also for example $^{19}F+^{12}C$ in Ref. [11]).

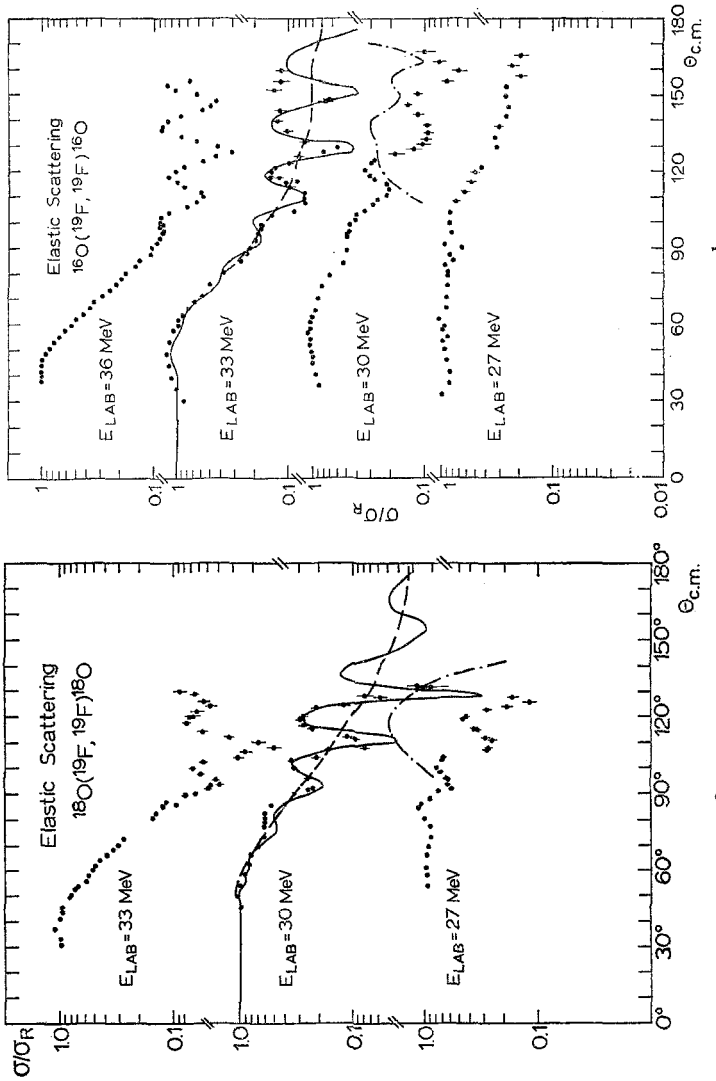

Fig. 14a and b. Non interfering and total cross sections for the systems $^{19}F+^{18}O$ and $^{19}F+^{16}O$

Differences in the angular distributions observed in the scattering with ^{18}O, ^{16}O and ^{15}N can quantitatively be described taking elastic transfer into account. Attempts to describe, in particular the $^{19}F+^{16}O$ system with an optical model with weak surface absorption gave no consistent description at the four energies measured. The energy variation of the angular distributions is, however, rather well described if the elastic transfer is taken properly into account. The effects of the elastic transfer are mainly observable at angles larger 90° CM (slightly depending on the bound state of the transferred particle) and usually are not easily detected if excitation functions at angles smaller 90° CM are considered. The exchange of three (one) nucleons in the scattering of ^{19}F on $^{16}O(^{19}F+^{18}O)$ and two neutrons of ^{18}O on ^{16}O [10, 19] are responsible for the deviations from the strong absorption scattering observed in these systems. The coherent addition of an elastic transfer cross section which is app. 1/10 of the elastic cross section gives rise to the oscillatory structure observed at large angles (Fig. 14 gives illustrations). From the analysis of the three systems in the present work, $^{19}F+^{18}O$, $^{19}F+^{16}O$ and $^{15}N+^{19}F$ the parentage for the decomposition of ^{19}F into proton$+^{18}O$ or triton$+^{16}O$ or α-particle$+^{15}N$ has been deduced. The values of the spectroscopic factors, which were found to describe the correct strength of the elastic transfer are in very good agreement with values deduced from other transfer reactions.

The authors thank Prof. U. Schmidt-Rohr and Prof. R. Bock for their interest in this work. They thank Dr. Marquardt and Mr. Gebauer for their assistance during part of this work. Special thanks are due to Mr. Schmidt and Mr. Koeßler and their crew for their efforts in preparing the heavy ion beams.

References

1. Symposium on Heavy Ion Scattering, Argonne, 1971, ANL-7837.
2. Siemssen, R. H.: Elastic and inelastic scattering of heavy ions, chapter IV, C, 1 of nuclear spectroscopy, II ed. by J. Cerny. Academic Press, in preparation.
3. Chatwin, R. A., Eck, J. S., Robson, D., Richter, A.: Phys. Rev. C **1**, 795 (1970).
4. Gobbi, A., Matter, U., Perrenoud, J. L., Marmier, P.: Nucl. Phys. A **112**, 537 (1970).
5. Oertzen, W. von, Gutbrod, H.-H., Müller, M., Voos, U. C., Bock, R.: Phys. Lett. **26** B, 291 (1968).
6. Oertzen, W. von: Nucl. Phys. A **148**, 529 (1970).
7. Described in Hildenbrand, K. D., Gutbrod, H. H., Oertzen, W. von, Bock, R.: Nucl. Phys. A **157**, 297 (1970).
8. Gebauer, B., Bohlen, H. G., Oertzen, W. von, Kohlmeyer, B., Habib, E. E., Marquardt, N.: to be published.
9. Bohlen, H. G., Gebauer, B., Marquardt, N., Oertzen, W. von, Habib, E. E., Kohlmeyer, B.: J. Physique C **6**, 141 (1971).

10. Siemsen, R. H., Fortune, H. T., Richter, A., Tippie, J. W.: Phys. Rev. C **5**, 1839 (1972).
11. Voos, U. C., Oertzen, W. von, Bock, R.: Nucl. Phys. A **135**, 207 (1969).
12. Shaw, R. W., Vandenbosch, R., Mehta, M. K.: Phys. Rev. Letters **25**, 457 (1970).
13. Oertzen, W. von, Nörenberg, W.: Nucl. Phys. in press.
14. Bohlen, H. G., Oertzen, W. von: Phys. Lett. J 7 B, 451 (1971).
15. Fuller, R. C., McVoy, K. W.: Phys. Lett. **41** B, 257 (1972).
Oertzen, W. von, Nörenberg, W.: to be published in Nucl. Phys.
16. Schmid, C., Duhm, H. H.: Nucl. Phys. A **155**, 644 (1970).
17. Green, L. L., Lennon, C. O., Naqib, I. M.: Nucl. Phys. A **142**, 137 (1970).
18. Kubo, K. I.: Nucl. Phys. A **187**, 205 (1972).
19. Gelbke, C. K., Bock, R., Braun-Munzinger, P., Fick, D., Hildenbrand, K. D., Richter, A., Weiß, W.: Phys. Rev. Letters **29**, 1683 (1972).

H. G. Bohlen
M. Feil
A. Gamp
Max-Planck-Institut für Kernphysik
D-6900 Heidelberg
Postfach 1248
Federal Republic of Germany

N. Marquardt
Laboratoire de Physique Nucléaire
Université de Montréal
Case postale 6128
Montréal 101, Canada

W. v. Oertzen
Lawrence Radiation Laboratory
Berkeley, Calif., USA

R. L. Walter
Duke University
Durham, North Carolina, USA